Ore Geology Reviews 102 (2018) 811–817

Contents lists available at ScienceDirect

Ore Geology Reviews

journal homepage: www.elsevier.com/locate/oregeorev

Mapping mineral prospectivity through big data analytics and a deep learning algorithm

Yihui Xiong[a], Renguang Zuo[a,*], Emmanuel John M. Carranza[b]

[a] State Key Laboratory of Geological Processes and Mineral Resources, China University of Geosciences, Wuhan 430074, China
[b] University of KwaZulu-Natal, Westville Campus, Durban, South Africa

ARTICLE INFO

Keywords:
Big data
Deep learning
Mapping mineral prospectivity
GIS

ABSTRACT

Identification of anomalies related to mineralization and integration of multi-source geoscience data are essential for mapping mineral prospectivity. In this study, we applied big data analytics and a deep learning algorithm to process geoscience data to identify and integrate anomalies related to skarn-type Iron mineralization in the southwestern Fujian metallogenic zone of China. Based on the geological setting and environment for the formation of skarn-type Iron mineralization, 42 relevant variables, including two geological, one geophysical, and 39 geochemical variables, were analyzed and integrated for detecting anomalies related to mineralization using a deep autoencoder network. The results indicate that the mapped prospectivity areas have a strong spatial relationship with the locations of known mineralization and demonstrate that big data analytics supported by deep learning methods is a potential technique to be considered for use in mineral prospectivity mapping.

1. Introduction

Prospecting for buried mineral deposits in covered regions remains to be one of the most critical but challenging issues in mineral exploration and resource assessment. There are various issues that have to be overcome for mineral exploration in these regions, such as indirect and weak geo-information related to buried deposits acquired from geophysical and geochemical surveys due to complex overprinting relationships arising from multiple geological processes, and incomplete and poor coverage of geo-information due to masking effects and/or sampling difficulties (Cheng, 2012). New theories and analytical methods are required for mapping, interpreting and integrating diverse geo-information to increase the success rate and reduce the costs of mineral exploration. From both a data science and mathematical geosciences perspective, extraction of geo-information that allows the location and exploration of buried mineralization deserves more attention from geoscientists. Particularly, as the amounts of high quality data from multiple sources covering a broad range of scales have recently become readily available.

The era of big data coincides with the exponential growth, availability, and usage of data and information (Reichman et al., 2011; Wang et al., 2016). The term “big data” does not only mean large datasets, but also refers to the characteristics of data itself, such as different kinds of formats and sources of data (Hu et al., 2014). The features of big data are intrinsic to the field of geosciences and have been recognized previously. The massive collection of earth observation data presents an unprecedented opportunity to apply big data approaches to solving problems in the geosciences (Gore, 1998; Goodchild, 2008; Deng and Di, 2009). The theory of big data not only provides for novel approaches to mineral exploration and assessment (Zuo and Xiong, 2018), but it can also be used to analyze, enhance and extract additional information from existing geosciences data (Wang et al., 2018a). The significance of applying big data approaches to mineral exploration is not only to generate a variety of anomaly maps using different kinds of big data, but also to identify the statistical and spatial characteristics of distribution, enrichment and depletion of metallogenic elements (Wang et al., 2015a). Big data analytics utilizes full samples, instead of partial samples, thus permitting a more detailed exploratory analysis of statistical correlations among all the available data (Mayer-Schonberger and Cukier, 2013). The core function of big data analytics is prediction, making it an ideal approach for predictive mapping of mineralized locations. For instance, Liu et al. (2016) used terrain elevation, slope, aspect, curvature, surface rolling, surface incision, terrain feature, and other kinds of landform factor values to calculate a terrain factor that distinguished mineral occurrence and mining areas. Further, they mapped the favorable geomorphic environment for hosting weathered crust-type rare earth mineralization in the eastern Nanling region using a variety of DEM-derived geomorphic

* Corresponding author.
E-mail address: zrguang@cug.edu.cn (R. Zuo).

https://doi.org/10.1016/j.oregeorev.2018.10.006
Received 8 May 2018; Received in revised form 26 September 2018; Accepted 11 October 2018
Available online 12 October 2018
0169-1368/

features. Luo et al. (2017) established a quantitative prediction model for Au mineralization based on integrated geophysical and geochemical datasets, demonstrating that big data analytics has the potential for mapping mineral prospectivity. Conventional methods used to map geochemical anomalies commonly focus on the detection of positive geochemical anomalies and ignore negative geochemical anomalies related to mineralization (Zuo and Xiong, 2018). Techniques of big data analytics techniques can overcome these limitations of by using the entire geochemical dataset to identify geochemical anomalies and quantify their statistical and spatial correlations with known mineralization patterns.

With the rapid developments in computing power, machine learning methods have been proven to be useful for big data analytics and knowledge discovery (Chen et al., 2014a). These methods mine data to analyze underlying patterns, thereby aiding in decision-making. Various machine learning methods have been used in the field of mineral prospectivity mapping in recent years (Carranza, 2017; Zuo, 2017), such as decision tree (Agterberg and Bonham-Carter, 1999; Reddy and Bonham-Carter, 1991), neural networks (Singer and Kouda, 1996; Harris et al., 2003; Porwal et al., 2003, 2004, 2006; Leite and Souza Filho, 2009; Xiong and Zuo, 2017), support vector machines (Zuo and Carranza, 2011; Abedi et al., 2012), random forest (Carranza and Laborte, 2015a,b, 2016; Rodriguez-Galiano et al., 2014, 2015; Gao et al., 2016; McKay and Harris, 2016; Zhang et al., 2016b; Hariharan et al., 2017), and isolation forest (Chen and Wu, 2018). Deep learning, a newly developed approach to machine learning, are representation-learning methods with multiple levels of representation, acquired by assembling simple but non-linear modules. The original input can be converted into a higher, slightly more abstract representation through the stacked modules (LeCun et al., 2015). With the composition of enough such transformations, very complex functions can be learned (Hinton et al., 2006; LeCun et al., 2015). Deep learning has been proven to be both a prominent breakthrough and an extremely powerful tool in various fields. In geosciences, deep learning is widely used in remote sensing data classification (Chen et al., 2014b; Zhang et al., 2016a; Kussul et al., 2017), in earthquake studies for waveform feature extraction (Valentine and Trampert, 2012; Ross et al., 2018), in atmospheric studies for typhoon forecast and ground-level PM2.5 estimation (Jiang et al., 2018; Li et al., 2017), in mineral exploration for geochemical anomaly identification (Xiong and Zuo, 2016; Moeini and Torab, 2017; Zuo and Xiong, 2018).

In this study, big data analytics and a deep autoencoder network (Hinton and Salakhutdinov, 2006; Xiong and Zuo, 2016) were used to learn and mine meaningful patterns from massive amounts of input data for mapping mineral prospectivity in the southwestern Fujian metalorganic zone of China. This machine learning approach is relevant in the context of exploration for buried mineralization for its ability to discover complex features needed for detection or classification from the raw data. The aim of this study is to demonstrate the effectiveness of big data analytics and deep learning methods for mapping mineral prospectivity in forest-covered areas.

2. Study area and methods

2.1. Study area

The southwestern Fujian metallogenic zone, located in the Yangtze and the Cathaysia block, is well-known for its extensive Mesozoic tectono-magmatic events and accompanying skarn-type iron polymetallic mineralization (e.g., Makeng, Luoyang, Zhongjia, and Pantian iron deposits). The majority of the iron deposits are distributed within the early Hercynian Yong'an–Meixian fold belt (Ge et al., 1981; Zhang et al., 2013, 2015a,b; Wang et al., 2018b). The Lower Carboniferous Lindi Formation (C_1l) and the Upper Carboniferous Jingshe Formation (C_2j) are the major host strata for the iron polymetallic mineralization (Han and Ge, 1983; Zhang and Zuo, 2014; Wang et al., 2015c; Zhang et al., 2015a,b; Zuo et al., 2015; Zuo, 2016).

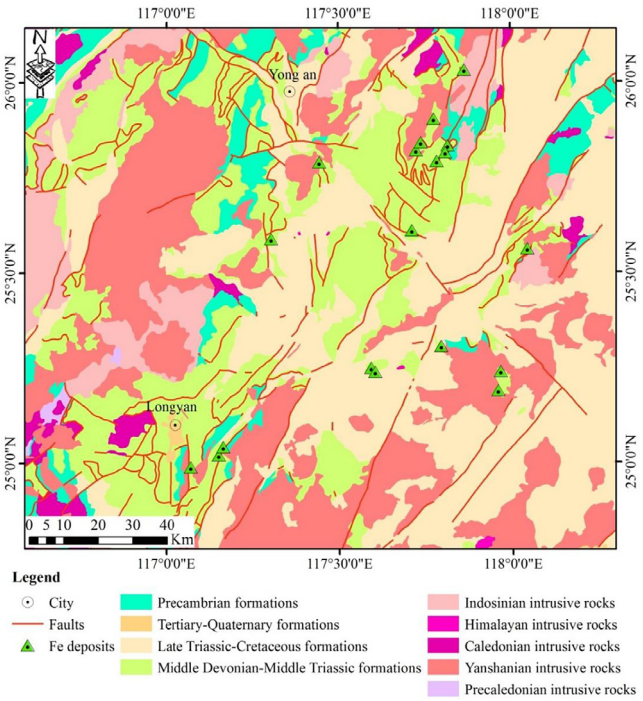

Fig. 1. Simplified geological map and the spatial distribution of Fe mineral deposits (Compiled from China Geological Survey).

The plutonic rocks in this region include Caledonian granitoids, Hercynian–Indosinian granitoids, and Yanshanian granitoids, which are classified by the different stages of the geological evolution of the region (Zhou and Li, 2000; Zhou et al., 2006; Mao, 2013). The zircon U–Pb dating ages of granitoids in Makeng region (Dayang granites: 128–145 Ma, Zhang et al., 2012a; Juzhou granite: 132 Ma, Wang et al., 2015b), Luoyang (131–132 Ma, Zhang et al., 2012b), Pantian (131 Ma, Lai et al., 2014), and Zhongjia (99 Ma, Yang et al., 2008) have a close temporal and spatial relationship with iron polymetallic mineralization and Yanshanian intrusions. The three dominant structures mapped in the region, namely the NE-trending Zhenghe–Dafu Fault, the NW-trending Shanghang–Yunxiao Fault, and the NNE-trending Nanping–Ninghua Fault, together with spatially associated secondary faults, appear to have provided pathways for the transport of ore-forming fluid. In addition, the NE-trending Mesozoic nappe structures and fold belts that formed under compression during the early subduction of the paleo-Pacific plate are also important regional structures that are spatially associated with mineralization (Kuo et al., 2016; Wang et al., 2017) (Fig. 1).

2.2. Deep autoencoder network

The unsupervised deep autoencoder network (DAN) was used to map mineral prospectivity in this study. The DAN model can be used to encode and reconstruct a sample population. According to Chen (2015) and Xiong and Zuo (2016), small sample sizes (e.g., mineral deposit occurrences) usually have a low probability of detection, are poorly encoded and thus linked to high reconstruction errors in the DAN model. However, as mineralization is a special type of singularity event and can be considered a rare event (Xiong and Zuo, 2018), the number of prospective areas is considerably less than the number of non-prospective areas. Therefore, the high reconstructed errors associated with these low detection probability features can be used to distinguish prospective locations from non-prospective locations. The reconstructed errors can be obtained as:

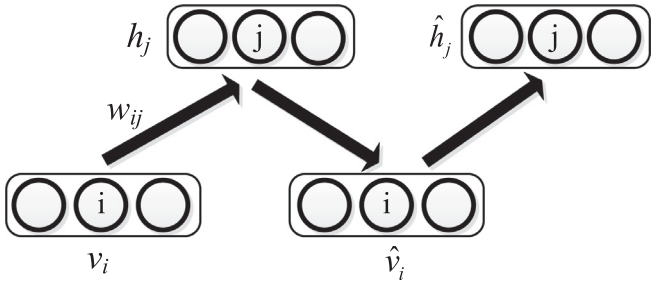

Fig. 2. The structure of Gibb's sampling and contrastive divergence for restrict Boltzmann machine training (revised from Hinton (2002)).

$$E = \sqrt{\sum_{i=1}^{n} (O_i - I_i)^2} \tag{1}$$

where E denotes the reconstructed error of each cell, and O_i is the reconstructed input data I_i. Three steps are involved in the training of the DAN. First, continuous restricted Boltzmann machines (CRBMs) are pretrained one by one for initialization of weights; then, all the trained CRBMs are stacked to construct a DAN, followed by fine-tuning via a back-propagation (BP) algorithm. The activation function of the DAN during the training can be defined as:

$$f(x_i) = \theta_L + (\theta_H - \theta_L) \cdot \frac{1}{1 + \exp(-x_i)} \tag{2}$$

where $f(x_i)$ represents the sigmoid function and the two constants θ_L and θ_H represent the asymptotes of $f(x_i)$.

The CRBMs are typically stochastic neural networks and are usually trained via minimizing contrastive divergence (MCD) learning rule (Hinton, 2002) (Fig. 2). Given the visible units (v_i), the hidden units (h_j) can be calculated as:

$$h_j = f\left(\sum_i w_{ij} v_i + b_j + \sigma N(0, 1)\right) \tag{3}$$

where w_{ij} represents the weight between visible and hidden units. A similar way can be used to calculate the visible units ($\hat{v}_i$), thus:

$$\hat{v}_i = f\left(\sum_j w_{ij} h_j + b_i + \sigma N(0, 1)\right) \tag{4}$$

where b_i represents the bias of the units. Thus, the weight w_{ij} can be updated as follows:

$$\Delta w_{ij} = \eta_w (\langle v_i h_j \rangle - \langle \hat{v}_i \hat{h}_j \rangle) \tag{5}$$

where η_w represents the learning rate of weight. $\hat{v}_i$ is the one-step reconstructed states of visible units and $\hat{h}_j$ is the one-step reconstructed states of hidden units.

All the trained CRBMs are stacked to construct a DAN and the BP algorithm with a gradient descent technique is introduced to fine-tune the parameters in the network to achieve minimal reconstructed errors (Hinton, 2002; Hinton and Salakhutdinov, 2006). The principle of mineral prospectivity mapping by reconstructed errors can be found in Chen (2015), and the calculation process of DAN for mineral prospectivity mapping is shown in Fig. 3.

3. Dataset and results

3.1. Data

The datasets used in this study comprise geological, geochemical, and geophysical data. The 1:200,000 scale geological map of the study area comprises intrusive rocks, sedimentary formations, faults, and iron deposits (Fig. 1). Stream sediment geochemical data, which were sampled at a density of 1 sample per 4 km^2, were compiled from the Chinese National Geochemical Mapping project (Xie et al., 1997). Geophysical data consist of airborne total magnetic intensity data sampled at 2 km spatial resolution, provided by the China Geological Survey (CGS). The following variables were identified as suitable predictors of prospectivity based on previous geological studies and the mineral system model for the formation of skarn-type iron-related mineralization (Zhang and Zuo, 2014; Zhang et al., 2015a,b, 2016b; Zuo et al., 2015).

3.1.1. Carbonate rocks and granites

The Yanshanian granites and Carboniferous–Permian carbonate formations (Fig. 4a) play important roles in the formation of iron mineralization in the district. The former provided the heat and metallogenic fluids for iron mineralization, and the latter provided a depositional host for ore-forming elements due to their strong chemical reactivity, brittleness, and high permeability (Zhang et al., 2016b).

3.1.2. Faults

The NE- and NNE-trending faults in the region are believed to have provided pathways for the transportation of magmatic-hydrothermal fluids. Therefore, a 10-ring buffer was constructed around these faults with an interval distance of 1 km (Zhang et al., 2016b) (Fig. 4b).

3.1.3. Geochemical anomalies

Geochemical anomalies are related to both the iron mineralization and skarn alteration. This type of mineralization was formed by complex geochemical processes, with many geochemical elements from both the host and source rocks involved in water–rock interactions, leading to complex geochemical patterns (Zuo and Xiong, 2018). Therefore, all 39 elements measured by the China geochemical mapping program were considered in this study. Further detailed information about the data including sampling, analysis, detection limit, and quality can be found in Xie et al. (1997). The geochemical dataset used in this study has been successfully used for mapping geochemical anomalies associated with iron mineralization (Zuo, 2018; Zuo and Xiong, 2018). Fig. 4c shows the spatial distribution of the singularity indices of Fe_2O_3, which were generated through inverse distance weighted (IDW) interpolation with a cell size of 1 km × 1 km followed by local singularity analysis (Cheng, 2007; Zuo et al., 2009, 2016) for identification of geochemical anomalies. The same steps were followed to preprocess data for the other 38 geochemical elements.

3.1.4. Aeromagnetic anomaly

Skarn-type Fe deposits in this district have obvious aeromagnetic anomaly according to its physical property, which can be considered as direct detectors of Fe-related mineralization (Zhang et al., 2016b). Three steps were followed to model the aeromagnetic anomaly, namely spatial interpolation by IDW using a 1 km cell size, reducing to the geomagnetic role by transforming oblique magnetization to vertical magnetization, and local singularity analysis to derive the final aeromagnetic anomaly (Fig. 4d).

3.2. Results

GIS rasters with cell size of 1 km × 1 km were created for all 42 variables, which include two geological, one geophysical, and 39 geochemical variables. The maps were combined into a set of input feature vectors for detecting anomalies related to mineralization using DAN. In this experiment, the DAN was stacked with four CRBMs, and the general case, namely, the size of different layers in terms of decreasing it (halves) with the increase of layer index was conducted to the number of hidden units. The results confirm that the reconstruction error stabilizes at the number of 240, thus a 128-64-32-16-32-64-128 autoencoder network was set (Fig. 5a).

For mapping mineral prospectivity, the DAN contains four hidden

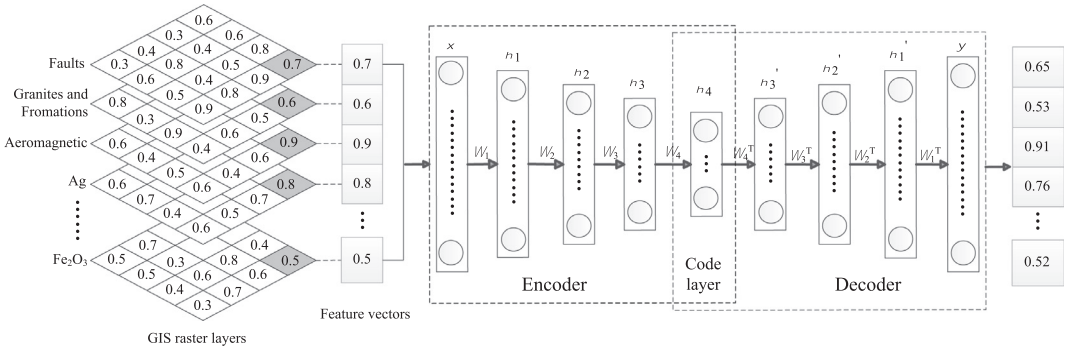

Fig. 3. The calculation process of deep autoencoder network.

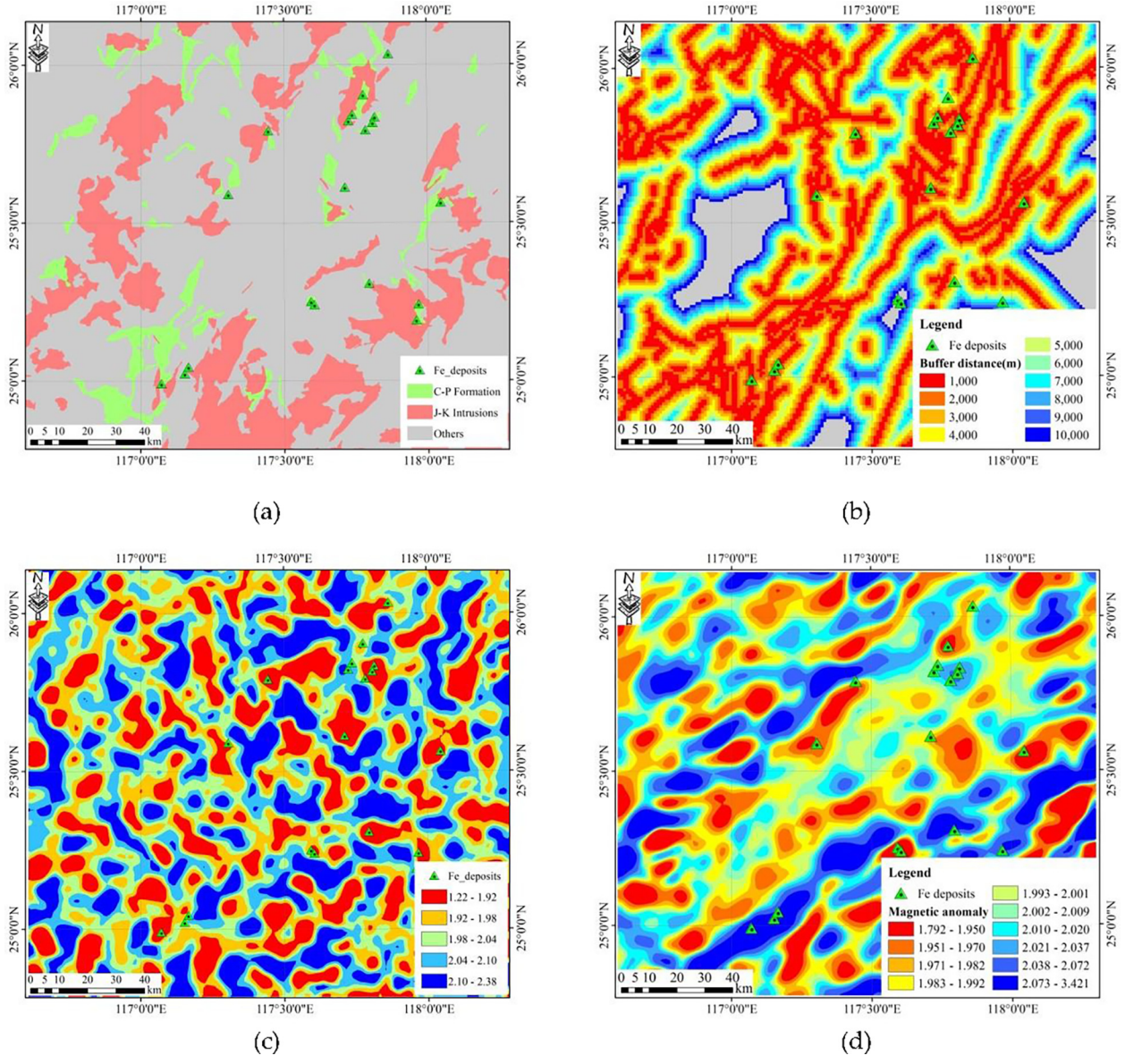

Fig. 4. Maps showing the spatial distribution of (a) favorable formation and intrusions, (b) faults, (c) geochemical anomalies for Fe_2O_3, and (d) aeromagnetic anomalies.

layers and the corresponding units of the hidden layers are 128-64-32-16. Due to the symmetrical characteristic of the DAN, a 128-64-32-16-32-64-128 autoencoder network was built. The average reconstruction error reaches a minimum and keeps stable at 300 epochs, thus the number of iterations was set to 300 to generate a well-trained network (Fig. 5b). The other parameters, such as the weight-cost and learning moment, are set to 0.00001 and 0.9 based on expert opinion (Hinton, 2012). The high prospectivity values mapped by the DAN technique

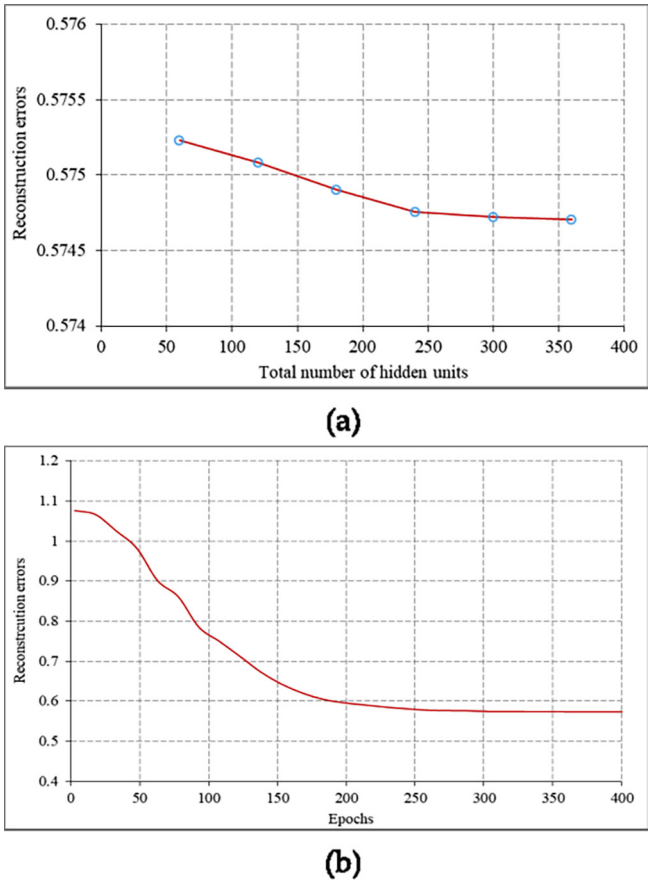

Fig. 5. (a) Reconstruction error for decrease architectures, as a function of the total number of hidden units; (b) Average reconstruction error varying with training cycles.

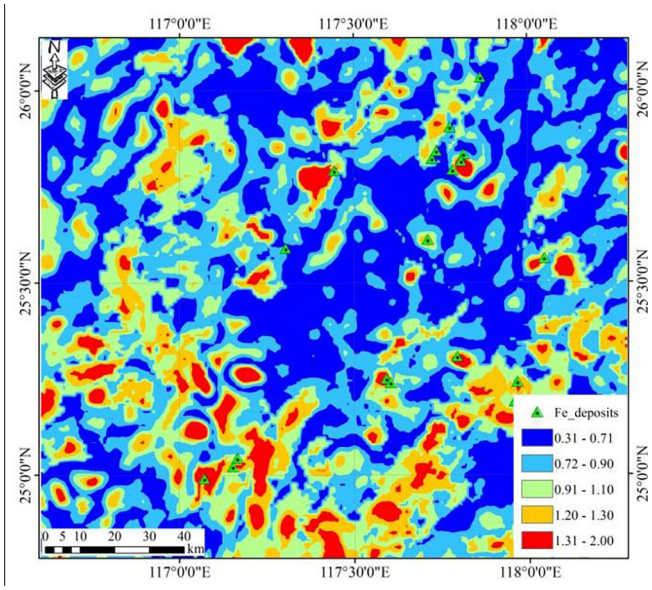

Fig. 6. Map showing the detected anomalies related to Fe-related mineralization.

(Fig. 6) have a strong spatial relationship with the locations of known mineral deposits, which is confirmed statistically by the areas under curve of the receiver operating characteristic curve being greater than 0.75 (Fig. 7). This indicates that a big data approach can be used for integrating multi-source geoscience data and spatial decision-making

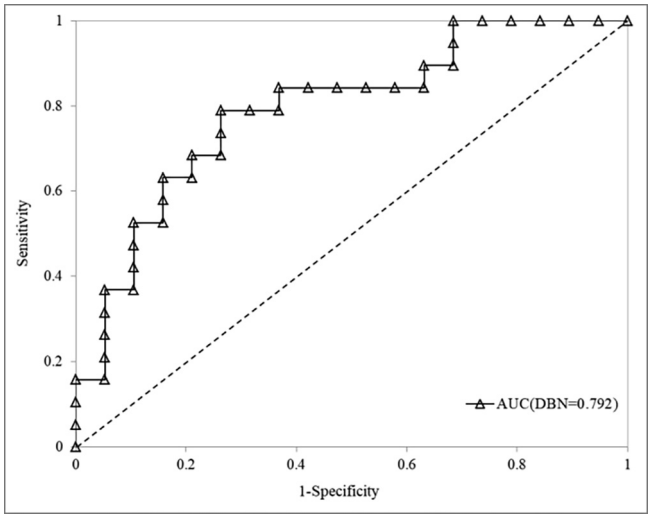

Fig. 7. ROC curve.

supported by deep learning methods.

4. Discussion and conclusions

The concepts behind big data analytics are that (1) the technique use full samples rather than partial samples, (2) the technique statistical correlations rather than causal relations among all available data, and (3) the technique is based on data science, and lets the data speak for themselves (Mayer-Schonberger and Cukier, 2013). These three concepts of big data analytics are beneficial for exploring spatial correlations between geological features and presence of mineralization and integrating multi-source data. In the context of mineral prospectivity mapping, big data analytics can map potential locations of mineralization since the technique's core function is prediction. Therefore, it is expected to be a new and effective approach for mapping mineral prospectivity.

Traditional deep multilayer neural networks are generally not successfully trained, mainly because the training algorithm, standard gradient decent from random initialization, performs poorly in multilayer neural networks (Rumelhart et al., 1988; Larochelle et al., 2009; Glorot and Bengio, 2010). Compared to traditional neural networks, deep learning algorithms use different initialization and training schemes, such as unsupervised pre-training and fine-tuning strategies. This enables better high-level extraction of complex features and data representations from large volumes of data and makes it a powerful tool for big data analytics (Glorot and Bengio, 2010; Najafabadi et al., 2015). These advantages indicate that deep learning methods can be effectively used for identifying geological anomalies and patterns (Xiong and Zuo, 2016).

The advantages of big data analytics and deep learning algorithms are that (1) they can deal with complex problems and identify hidden spatial patterns, which are difficult for traditional methods of mapping mineral prospectivity, and (2) they utilize existing datasets to derive correlations between geological features and mineral deposits, thereby overcoming the disadvantages of the need to use subjective models that contain experts' bias. However, the scale and number of variables required for mapping mineral prospectivity via big data analytics and deep learning algorithms, can lead to data dimension problem, computing complexity, and data redundancy. Furthermore, the results are difficult to interpret from a geological perspective because the deep learning method lacks transparency. This can make it difficult for geologists to be confident in the prospectivity mapping results from big data analytics and deep learning algorithms. Therefore, significant effort is required for mathematical geoscientists to develop a deep

learning model with an accessible and transparent structure to bridge the communication gap between geologists and data scientists.

The hybrid method of big data analytics and deep learning algorithms provides a novel and powerful tool for the identification of geological anomalies and integration of multi-layer geoscience datasets. The case study of mapping iron mineralization in the southwestern Fujian metalorganic zone of China demonstrates the effectiveness of such a hybrid method for mineral prospectivity mapping. However, studies on geological settings and mineral deposit models are also needed because they provide geological constraints and help identify the relevant geoscience data to be mapped. In addition, in this study, only geological, geochemical, and geophysical datasets were used. However, there are various remote sensing datasets that could potentially be incorporated. The questions of how to choose relevant datasets and incorporate them into the existing dataset for mapping mineral prospectivity should be further explored.

Acknowledgments

We thank Greg Partington and an anonymous reviewer for their valuable comments and suggestions, which helped us improve the presentation of material in this study. This research was jointed supported by the National Key Research and Development Program of China under Grant 2016YFC0600508, the National Natural Science Foundation of China under Grants 41372007 and 41522206, the Natural Science Foundation of Hubei Province (China) under Grant 2017CFA053, and Open Research Project of The Key Laboratory of Intelligent Geo-Information Processing 295 under Grant KLIGIP-2017A03.

References

Abedi, M., Norouzi, G.H., Bahroudi, A., 2012. Support vector machine for multi-classification of mineral prospectivity areas. Comput. Geosci. 46, 272–283.
Agterberg, F.P., Bonham-Carter, G.F., 1999. Logistic regression and weights of evidence modeling in mineral exploration. In: Proceedings of the 28th International Symposium on Applications of Computer in the Mineral Industry (APCOM), Golden, Colorado, pp. 483–490.
Carranza, E.J.M., 2017. Natural Resources Research publications on geochemical anomaly and mineral potential mapping, and introduction to the special issue of papers in these fields. Nat. Resour. Res. 26, 379–410.
Carranza, E.J.M., Laborte, A.G., 2015a. Data-driven predictive mapping of gold prospectivity, Baguio district, Philippines: application of random forests algorithm. Ore Geol. Rev. 71, 777–787.
Carranza, E.J.M., Laborte, A.G., 2015b. Random forest predictive modeling of mineral prospectivity with small number of prospects and data with missing values in Abra (Philippines). Comput. Geosci. 74, 60–70.
Carranza, E.J.M., Laborte, A.G., 2016. Data-driven predictive modeling of mineral prospectivity using random forests: a case study in Catanduanes Island (Philippines). Nat. Resour. Res. 25, 35–50.
Chen, M., Mao, S., Liu, Y., 2014a. Big data: a survey. Mobile Networks Appl. 19, 171–209.
Chen, Y., 2015. Mineral potential mapping with a restricted Boltzmann machine. Ore Geol. Rev. 71, 749–760.
Chen, Y., Lin, Z., Zhao, X., Wang, G., Gu, Y., 2014b. Deep learning-based classification of hyperspectral data. IEEE J. Sel. Top. Appl. Earth Obs. Remote Sens. 7, 2094–2107.
Chen, Y., Wu, W., 2018. Isolation forest as an alternative data-driven mineral prospectivity mapping method with a higher data-processing efficiency. Nat. Resour. Res. https://doi.org/10.1007/s11053-018-9375-6.
Cheng, Q., 2007. Mapping singularities with stream sediment geochemical data for prediction of undiscovered mineral deposits in Gejiu, Yunnan Province, China. Ore Geol. Rev. 32, 314–324.
Cheng, Q., 2012. Singularity theory and methods for mapping geochemical anomalies caused by buried sources and for predicting undiscovered mineral deposits in covered areas. J. Geochem. Explor. 122, 55–70.
Deng, M., Di, L., 2009. Building an online learning and research environment to enhance use of geospatial data. Int. J. Spatial Data Infrastruct. Res. 4, 77–95.
Gao, Y., Zhang, Z., Xiong, Y., Zuo, R., 2016. Mapping mineral prospectivity for Cu polymetallic mineralization in southwest Fujian Province, China. Ore Geol. Rev. 75, 16–28.
Ge, C., Han, F., Zhou, T., Chen, D., 1981. Geological characteristics of the Makeng iron deposit of marine volcano-sedimentary origin. Acta Geosci. Sin. 3, 47–69 (in Chinese with English Abstract).
Glorot, X., Bengio, Y., 2010. Understanding the difficulty of training deep feedforward neural networks. In: Proceedings of the thirteenth international conference on artificial intelligence and statistics, pp. 249–256.
Goodchild, M.F., 2008. The use cases of digital earth. Int. J. Digital Earth 1, 31–42.
Gore, A., 1998. The digital earth: understanding our planet in the 21st century. Aust. Surv. 43, 89–91.
Han, F., Ge, C., 1983. Geological and geochemical features of submarine volcanic hydrothermal-sedimentary mineralization of Makeng iron deposit, Fujian Province. Bull. Inst. Miner. Deposits Chin. Acad. Geol. Sci. 7, 1–118 (in Chinese with English abstract).
Hariharan, S., Tirodkar, S., Porwal, A., Bhattacharya, A., Joly, A., 2017. Random forest-based prospectivity modelling of greenfield terrains using sparse deposit data: an example from the tanami region, western Australia. Nat. Resour. Res. 26, 489–507.
Harris, D.P., Zurcher, L., Stanley, M., Marlow, J., Pan, G., 2003. A comparative analysis of favourability mappings by weights of evidence probabilistic neural networks, discriminant analysis, and logistic regression. Nat. Resour. Res. 12, 241–255.
Hinton, G.E., 2002. Training products of experts by minimizing contrastive divergence. Neural Comput. 14, 1771–1800.
Hinton, G.E., 2012. A practical guide to training restricted Boltzmann machines. Neural Networks: Tricks of the Trade. Springer, Berlin, Heidelberg.
Hinton, G.E., Osindero, S., Teh, Y.-W., 2006. A fast learning algorithm for deep belief nets. Neural Comput. 18, 1527–1554.
Hinton, G.E., Salakhutdinov, R.R., 2006. Reducing the dimensionality of data with neural networks. Science 313, 504–507.
Hu, H., Wen, Y., Chua, T.S., Li, X., 2014. Toward scalable systems for big data analytics: a technology tutorial. IEEE Access 2, 652–687.
Jiang, G.Q., Xu, J., Wei, J., 2018. A deep learning algorithm of neural network for the parameterization of typhoon-ocean feedback in typhoon forecast models. Geophys. Res. Lett. 45, 3706–3716.
Kuo, Y., Wang, C., Kuo-Chen, H., Jin, X., Cai, H., Lin, J., Wu, F.T., Yen, H., Huang, B., Liang, W., Okaya, D., Brown, L., 2016. Crustal structures from the Wuyi-Yunkai orogen to the Taiwan orogen: the onshore-offshore wide-angle seismic experiments of the TAIGER and ATSEE projects. Tectonophysics 692, 164–180.
Kussul, N., Lavreniuk, M., Skakun, S., Shelestov, A., 2017. Deep learning classification of land cover and crop types using remote sensing data. IEEE Geosci. Remote Sens. Lett. 14, 778–782.
Lai, S., Chen, R., Zhang, D., Di, Y., Gong, Y., Yuan, Y., Chen, L., 2014. Petrogeochemical features and zircon LA-ICP-MS U-Pb ages of granite in the Pantian iron ore deposit, Fujian province and their relationship with mineralization. Acta Petrol. Sin. 30, 1780–1792 (in Chinese with English abstract).
Larochelle, H., Bengio, Y., Louradour, J., Lamblin, P., 2009. Exploring strategies for training deep neural networks. J. Mach. Learn. Res. 10, 1–40.
LeCun, Y., Bengio, Y., Hinton, G., 2015. Deep learning. Nature 521, 436–444.
Leite, E.P., Souza Filho, C.R., 2009. Probabilistic neural networks applied to mineral potential mapping for platinum group elements in the Serra Leste region, Carajás Mineral Province, Brazil. Comput. Geosci. 35, 675–687.
Li, T., Shen, H., Yuan, Q., Zhang, X., Zhang, L., 2017. Estimating ground-level PM2. 5 by fusing satellite and station observations: a geo-intelligent deep learning approach. Geophys. Res. Lett. 44, 11985–11993.
Liu, X., Chen, Y., Wang, D., Huang, F., Zhao, Z., 2016. The Metallogenic geomorphic rare earths ore in the eastern nanling region based on DEM data. Acta Geosci. Sin. 37, 174–184 (In Chinese with English abstract).
Luo, J., Zhang, Q., Song, B., Wang, X., Yang, Z., Zhao, Y., Liu, S., 2017. Application of integrated geophysical and geochemical data processing to metallogenic target zone quantitative prediction and optimization. Bull. Mineral. Petrol. Geochem. 36, 886–890 (In Chinese with English abstract).
McKay, G., Harris, J.R., 2016. Comparison of the data-driven Random Forests model and a knowledge-driven method for mineral prospectivity mapping: a case study for gold deposits around the Huritz Group and Nueltin Suite, Nunavut, Canada. Nat. Resour. Res. 25, 125–143.
Mao, J., 2013. Mesozoic-Cenozoic Magmatism and Mineralization in South China Block (SCB) and Adjacent Region. China science press (CSPM) (In Chinese with English abstract).
Mayer-Schonberger, V., Cukier, K., 2013. Big data: a revolution that will transform how we live, work and think. Houghton Mifflin Harcourt Publishing Company, New York.
Moeini, H., Torab, F.M., 2017. Comparing compositional multivariate outliers with autoencoder networks in anomaly detection at Hamich exploration area, east of Iran. J. Geochem. Explor. 180, 15–23.
Najafabadi, M.M., Villanustre, F., Khoshgoftaar, T.M., Naeem, S., Wald, R., Muharemagic, E., 2015. Deep learning applications and challenges in big data analytics. J. Big Data 2, 1.
Porwal, A., Carranza, E.J.M., Hale, M., 2004. A hybrid neuro-fuzzy model for mineral potential mapping. Math. Geol. 36, 803–826.
Porwal, A., Carranza, E.J.M., Hale, M., 2006. Bayesian network classifiers for mineral potential mapping. Comput. Geosci. 32, 1–16.
Porwal, A., Carranza, E.J.M., Hale, M., 2003. Artificial neural networks for mineral potential mapping. Nat. Resour. Res. 12, 155–171.
Reddy, R.K.T., Bonham-Carter, G.F., 1991. A decision-tree approach to mineral potential mapping in Snow Lake area, Manitoba. Can. J. Remote Sens. 17, 191–200.
Reichman, O.J., Jones, M.B., Schildhauer, M.P., 2011. Challenges and opportunities of open data in ecology. Science 331, 703–705.
Rodriguez-Galiano, V., Chica-Olmo, M., Chica-Rivas, M., 2014. Predictive modelling of gold potential with the integration of multisource information based on random forest: a case study on the Rodalquilar area, Southern Spain. Int. J. Geogr. Inf. Sci. 28, 1336–1354.
Rodriguez-Galiano, V., Sanchez-Castillo, M., Chica-Olmo, M., Chica-Rivas, M., 2015. Machine learning predictive models for mineral prospectivity: an evaluation of neural networks, random forest, regression trees and support vector machines. Ore Geol. Rev. 71, 804–818.
Ross, Z.E., Meier, M.A., Hauksson, E., 2018. P-wave arrival picking and first-motion

polarity determination with deep learning. J. Geophys. Res. Solid Earth 123. https://doi.org/10.1029/2017JB015251.
Rumelhart, D.E., Hinton, G.E., Williams, R.J., 1988. Learning Representations by Back-propagation Errors. MIT Press, Cambridge, MA, USA.
Singer, D.A., Kouda, R., 1996. Application of a feedforward neural network in the search for Kuruko deposits in the Hokuroku district, Japan. Math. Geol. 28, 1017–1023.
Valentine, A.P., Trampert, J., 2012. Data space reduction, quality assessment and searching of seismograms: autoencoder networks for waveform data. Geophys. J. Int. 189, 1183–1202.
Wang, C., Ma, X., Chen, J., Chen, J., 2018a. Information extraction and knowledge graph construction from geoscience literature. Comput. Geosci. 112, 112–120.
Wang, D., Liu, X., Liu, L., 2015a. Characteristics of big geodata and its application to study of minerogenetic regularity and minerogenetic series. Miner. Deposits 34, 1143–1154 (In Chinese with English abstract).
Wang, H., Xu, Z., Fujita, H., Liu, S., 2016. Towards felicitous decision making: an overview on challenges and trends of Big Data. Inf. Sci. 367, 747–765.
Wang, S., Zhang, D., Vatuva, A., Yan, P., Ma, S., Feng, H., Yu, T., Bai, Y., Di, Y., 2015b. Zircon U-Pb geochronology, geochemistry and Hf isotope compositions of the Dayang and Juzhou granites in Longyan, Fujian and their geological implications. Geochimica 44, 450–468 (In Chinese with English abstract).
Wang, S., Zhang, D., Wu, G., Vatuva, A., Di, Y., Yan, P., Feng, H., Ma, S., 2017. Late Paleozoic to Mesozoic extension in southwestern Fujian Province, South China: geochemical, geochronological and Hf isotopic constraints from basic-intermediate dykes. Geosci. Front. 8, 529–540.
Wang, S., Zhang, D., Wu, G., Li, X., Gao, X., Vatuva, A., Yuan, Y., Yu, T., Bai, Y., Fang, Y., 2018b. Late mesozoic tectonic evolution of Southwestern Fujian Province, South China: constraints from magnetic fabric, Zircon U-Pb geochronology and structural deformation. J. Earth Sci. 29, 391–407.
Wang, Z., Zuo, R., Zhang, Z., 2015c. Spatial analysis of Fe deposits in Fujian Province, China: implications for mineral exploration. J. Earth Sci. 26, 813–820.
Xie, X., Mu, X., Ren, T., 1997. Geochemical mapping in China. J. Geochem. Explor. 60, 99–113.
Xiong, Y., Zuo, R., 2016. Recognition of geochemical anomalies using a deep autoencoder network. Comput. Geosci. 86, 75–82.
Xiong, Y., Zuo, R., 2017. Effects of misclassification costs on mapping mineral prospectivity. Ore Geol. Rev. 82, 1–9.
Xiong, Y., Zuo, R., 2018. GIS-based rare events logistic regression for mineral prospectivity mapping. Comput. Geosci. 111, 18–25.
Yang, Z., Zhang, D., Feng, C., She, H., Li, J., 2008. SHRIMP zircon U-Pb dating of quartz porphyry from Zhongjia tin–polymetallic deposit in Longyan area, Fujian Province, and its geological significance. Miner. Deposits 27, 329–335 (in Chinese with English Abstract).
Zhang, C., Li, L., Zhang, C., Wang, J., 2012a. LA-ICP-MS Zircon U-Pb ages and Hf isotopic compositions of Dayang Granite from Longyan, Fujian Province. Geoscience 26, 434–444 (in Chinese with English abstract).
Zhang, D., Wu, G., Di, Y., Wang, C., Yao, J., Zhang, Y., Lv, L., Yuan, Y., Shi, J., 2012b. Geochronology of diagenesis and mineralization of the Luoyang iron deposit in Zhangping city, Fujian province and its geological significance. Earth Sci. 37, 1217–1231 (In Chinese with English abstract).
Zhang, D., Wu, G., Di, Y., Yu, X., Shi, Y., Zhang, X., Wang, Q., Huang, H., 2013. SHRIMP U-Pb zircon geochronology and Nd-Sr isotopic study of the Mamianshan group: implications for the Neoproterozoic tectonic development of southeast China. Int. Geol. Rev. 55, 730–748.
Zhang, L., Zhang, L., Du, B., 2016a. Deep learning for remote sensing data: a technical tutorial on the state of the art. IEEE Geosci. Remote Sens. Mag. 4, 22–40.
Zhang, Z., Zuo, R., 2014. Sr–Nd–Pb isotope systematics of magnetite: implications for the genesis of Makeng Fe deposit, southern China. Ore Geol. Rev. 57, 53–60.
Zhang, Z., Zuo, R., Cheng, Q., 2015a. The mineralization age of the Makeng Fe deposit, South China: implications from U-Pb and Sm-Nd geochronology. Int. J. Earth Sci. 104, 663–682.
Zhang, Z., Zuo, R., Cheng, Q., 2015b. Geological features and formation processes of the Makeng Fe deposit, China. Resour. Geol. 65, 266–284.
Zhang, Z., Zuo, R., Xiong, Y., 2016b. A comparative study of fuzzy weights of evidence and random forests for mapping mineral prospectivity for skarn-type Fe deposits in the southwestern Fujian metallogenic belt, China. Sci. China Earth Sci. 59, 556–572.
Zhou, X., Li, W., 2000. Origin of Late Mesozoic igneous rocks in Southeastern China: implications for lithosphere subduction and underplating of mafic magmas. Tectonophysics 326, 269–287.
Zhou, X., Sun, T., Shen, W., Shu, L., Niu, Y., 2006. Petrogenesis of Mesozoic granitoids and volcanic rocks in South China: a response to tectonic evolution. Episodes 29, 26–33.
Zuo, R., 2016. A nonlinear controlling function of geological features on magmatic–hydrothermal mineralization. Sci. Rep. 6, 27127.
Zuo, R., 2017. Machine learning of mineralization-related geochemical anomalies: a review of potential methods. Nat. Resour. Res. 26, 457–464.
Zuo, R., 2018. Selection of an elemental association related to mineralization using spatial analysis. J. Geochem. Explor. 184, 150–157.
Zuo, R., Carranza, E.J.M., 2011. Support vector machine: a tool for mapping mineral prospectivity. Comput. Geosci. 37, 1967–1975.
Zuo, R., Zhang, Z., Zhang, D., Carranza, E.J.M., Wang, H., 2015. Evaluation of uncertainty in mineral prospectivity mapping due to missing evidence: a case study with skarn-type Fe deposits in Southwestern Fujian Province, China. Ore Geol. Rev. 71, 502–515.
Zuo, R., Xiong, Y., 2018. Big Data Analytics of Identifying Geochemical Anomalies Supported by Machine Learning Methods. Nat. Resour. Res. 27, 5–13.
Zuo, R., Cheng, Q., Agterberg, F.P., Xia, Q., 2009. Application of singularity mapping technique to identify local anomalies using stream sediment geochemical data, a case study from Gangdese, Tibet, western China. J. Geochem. Explor. 101, 225–235.
Zuo, R., Carranza, E.J.M., Wang, J., 2016. Spatial analysis and visualization of exploration geochemical data. Earth Sci. Rev. 158, 9–18.